Characteristics of strong ground motions from the L'Aquila (M_w = 6.3) earthquake and its strongest aftershocks.

F. Pacor[1], G. Ameri[1], D. Bindi[1], L. Luzi[1], M. Massa[1], R. Paolucci[2] and C.Smerzini[2]

(1) Istituto Nazionale di Geofisica e Vulcanologia, Milano, Italy
(2) Dept. of Structural Engineering, Politecnico di Milano, Italy

Corresponding author:
Gabriele Ameri,
Istituto Nazionale di Geofisica e Vulcanologia
via Bassini 15, 20133 Milano, Italy
e-mail: ameri@mi.ingv.it

Version: 8 November 2010
Accepted for publication in: Bollettino di Geofisica Teorica ed Applicata

Abstract

Strong motion data during the L'Aquila seismic sequence, started on April 6 2009 at 01:32 am GMT (M_W 6.3), were mainly recorded by the Italian accelerometric network (*Rete Accelerometrica Nazionale*, RAN), operated by the Department of Civil Protection (DPC). Several records were obtained also by a temporary network installed the day after the mainshock by the Istituto Nazionale di Geofisica e Vulcanologia (INGV Mi-Pv).

The L'Aquila earthquake is the third strongest seismic event producing strong-motion records in Italy, after the Irpinia (1980, M_W 6.9) and Friuli (1976, M_W 6.4) earthquakes. This event, together with the its largest aftershocks (M_W > 4.0) provided a unique strong-motion dataset in Italy, especially due to the amount and intensity of near-fault records. The dataset included in the Italian strong motion database, ITACA, consists of about 300 digital accelerograms (270 of which belonging to RAN), with a very good signal-to-noise ratio, recorded by about 70 stations, installed on different site conditions at distance ranging from 0 to 300 km. The national and international relevance of this dataset is enhanced by its contribution to fill gaps in the magnitude-distance distribution of worldwide strong motion records, especially for normal-fault earthquakes (Ameri et al., 2009). Near-fault records were obtained by (i) an array of 6 stations installed by DPC in 2001 in the Aterno Valley to study seismic site effects; (ii) station AQK close to downtown L'Aquila; (iii) station AQU, belonging to the broad-band Mednet network (mednet.rm.ingv.it/data.php), located in the L'Aquila historic castle; (iv) the stations of the INGV temporary network, installed in the epicentral region one day after the mainshock. These stations are located less than 5 km distance from the mainshock epicenter and are inside the surface projection of the fault rupture. This work presents an overview of the main features of seismic ground shaking during the L'Aquila sequence, referring to records of the mainshock and of the two strongest aftershocks. The dependence of the strong-motion parameters on distance, azimuth and site conditions as well as the characteristics of near-fault strong-motion records are discussed.

1. Introduction

On April 6, 2009, at 1:32:40 GMT, a Mw 6.3 earthquake struck the L'Aquila city, one of the largest urban centers in the Abruzzo region (Central Italy) with about 70,000 inhabitants, causing about 300 deaths and vast destructions in the town and surrounding villages.

The earthquake occurred along a NW-SE trending normal fault, 15-18 km long, dipping about 45° SW. The hypocenter depth was estimated at 9.5 km, and the epicenter at less than 5 km southwest to the town center (Chiarabba et al., 2009). The causative fault of the mainshock is associated with the tectonic depression of the Aterno river valley, sited between two main calcareous ridges, the Velino – Sirente to the southwest and the Gran Sasso to the north-northeast. The maximum observed intensity is IX-X in the MCS scale and the most relevant damages are distributed in NW-SE direction, with evident predominance towards SE (Galli and Camassi, 2009; Ameri et al., 2010). Accordingly to the normative for the Italian territory, the area struck by the L'Aquila earthquake is classified as a zone characterized by high level of seismic hazard (Gruppo di Lavoro MPS, 2004). In terms of probabilistic hazard assessment, the maximum peak ground acceleration having the probability of 10% of being exceeded in 50 years is 255 cm/s^2.

This event represents the third largest earthquake recorded by strong-motion instruments in Italy, after the 1980, M_w 6.9, Irpinia and the 1976, M_w 6.4, Friuli earthquakes (Luzi et al.; 2008).

The mainshock was followed, within the first week, by seven aftershocks with moment-magnitude greater than or equal to 5, the two strongest ones occurred on April 7th (Mw=5.6) and April 9th (Mw=5.4). The seismic sequence has been recorded by several digital stations of the Italian Strong-Motion Network (*Rete Accelerometrica Nazionale*, RAN), operated by the Italian Department of Civil Protection (DPC), by the Italian Seismometric Network (*Rete Sismometrica Nazionale*, operated by INGV-CNT; http://cnt.rm.ingv.it), and by a temporary strong-motion array installed by the INGV MI-PV (http://www.mi.ingv.it). Presently, the ITalian ACcelerometric Archive (ITACA), the new Italian strong motion database (http://itaca.mi.ingv.it), includes more than 900 waveforms from the L'Aquila earthquake sequence, including the M > 4 aftershocks occurred before April, 13th.

Strong motion data in near source regions were recorded by six accelerometric stations installed in 2001 by the DPC, across the upper Aterno valley and by four INGV MI-PV temporary stations sited close to the villages mainly damaged during the mainshock. Although some of these stations either

did not trigger or malfunctioned during the events, recordings from the array and the temporary network, together with the AQK and AQU stations located close to L'Aquila downtown, provide a near-fault strong-motion data set never recorded to date in Italy for events with M > 5, and one of the few ones worldwide.

This work presents an overview of the main features of seismic ground motion during the L'Aquila sequence, referring to records of the mainshock and of the two strongest aftershocks. The dependence of the strong-motion parameters on distance, azimuth and site conditions is discussed, as well as the characteristic of near-fault strong motion records in terms of amplitude and frequency content.

2. Strong Motion data set and site classification

In this work, we analyzed 136 recordings from strong-motion stations, extracted by the Italian Strong Motion Database ITACA (http://itaca.mi.ingv.it), triggered by the April 6, 2009, L'Aquila earthquake (hereinafter referred as event 1) and by the two largest aftershocks (2009/04/07 17:47:37, M_W 5.6 and 2009/04/09 00:52:59, M_W 5.4, hereinafter referred as event 2 and event 3, respectively). Figure 1 shows the location of the epicenters and of the closest recording stations, together with the focal mechanisms of the three events. Table 1 and Table 2 list the source parameters of the events and the main information of the stations up to 100 km from the relative epicenters.

The RAN stations are equipped with three-component sensors set to 1 or 2 g full-scale, coupled with 24-bit digitizers with a sampling rate of 200 S/s. The accelerographs of the four INGV Mi-Pv temporary stations were equipped with both an accelerometer (Kinemetrics Episensor ES-T) and a seismometer (either Lennartz 3D-5s or 3DLite) connected to a Reftek130 6 channel digitizer with a sampling rate of 100 S/s.

The recorded waveforms were processed following the new ITACA procedure (Paolucci et al., 2010), which consists in: removal of the linear trend fitting the entire record; application of a cosine taper and of a 2nd order acausal frequency-domain Butterworth filter to acceleration time series;

double integration to obtain displacement time series; linear de-trending of displacement; double-differentiation of displacement to get the corrected acceleration. Both the high-pass and low-pass filter corners were selected through visual inspection of the Fourier spectrum. The typical band-pass frequency range is between 0.1 and 25 to 40 Hz; the lower values of the high-cut off frequency have been selected for the stations far away from the epicenter (epicentral distance, R_{epi} > 100 km).

The sites were classified according to the Eurocode 8 (EC8; CEN, 2004) and the Italian Building Code (NTC08, 2008), based on the shear-wave velocity averaged over the top 30 m of the soil profile - Vs30 (where EC8 class A: Vs30 > 800 m/s, class B: Vs30=360-800 m/s, class C: Vs30 =180-360 m/s, class D: Vs30 <180 m/s and class E: 5 to 20 m of C- or D-type alluvium underlain by stiffer material with Vs > 800 m/s). The class of each station has been attributed on the basis of direct measure of $V_{s,30}$ or on geological/geophysical information (S4 project – http://esse4.mi.ingv.it – Deliverable D4, 2009).

The epicentral area corresponds to the upper and middle Aterno valley, which is characterized by a complex tectonic evolution reflected by the high variability of the geologic and geomorphologic patterns (Figure 2a). The valley is superimposed on a Quaternary lacustrine basin of tectonic origin. The depth of the Quaternary deposits is variable, from about 60m in the upper Aterno valley to more than 200m in the middle Aterno valley (Bosi et al., 2003). L'Aquila lies on a fluvial terrace, some tens of meters thick, consisting of calcareous breccias and conglomerates with limestone boulders and clasts in a marly matrix. The terrace lies on the top of lacustrine sediments, mainly consisting of silty and sandy layers and minor gravel beds (De Luca et al., 2005). As shown in Figure 2a, the terrace is at the left bank of the Aterno river valley, which flows about 50 m below downtown L'Aquila.

Due to the complexity of the area, the ground motion is expected to be substantially affected by local geological conditions. The site amplification effects for some of the considered strong motion stations have been recently spectrally investigated using strong motion recordings from 13 earthquakes of the L'Aquila seismic sequence with M > 4.0 (Bindi et al., 2009a). In particular,

high-frequency amplifications were detected for sites in class B (e.g., Antrodoco, ANT), whereas amplification peaks at frequencies close to or smaller than 1 Hz are identified for class C (e.g., Norcia, NOR).

The site responses at the stations belonging to the Aterno-valley array were also analyzed by Ameri et al. (2009) through the computation of the horizontal-to-vertical spectral ratios, HVSRs, (Lermo and Chavez-Garcia, 1993). Figure 2b shows the average HVSR plus/minus one standard deviation as well as horizontal and vertical site responses estimated through the generalized inversion technique by Bindi et al. (2009a) for some stations of the Aterno valley array and for AQK and AQU.

In general, all sites are characterized by no-flat HVSRs: broadband amplification is found for rock sites (AQP, AQG) while the stations installed on Quaternary deposits of the upper Aterno Valley (AQA, AQV, AQK, AQU) show remarkable amplifications at specific frequencies. In particular, AQK, located in the centre of L'Aquila town has a strong amplification peak at low frequency (about 0.6 Hz), as also demonstrated by De Luca et al. (2005) using weak motion and ambient noise data. This peak is also observed at AQU station but lower in amplitude.

3. Characteristics of the peak ground motions

The magnitude-distance distribution of the selected recordings is shown in Figure 3a, grouping the data according to the site conditions. We used the Joyner-Boore distance (R_{JB}), which is the shortest horizontal distance from the surface projection of the fault rupture, for the main event, and the epicentral distance (R_{epi}) for the two aftershocks since we do not have precise information on the location and dimension of the fault rupture. Note that this is a common assumption in ground motion prediction equations for magnitude smaller than about 5.5 (e.g., Akkar and Bommer, 2007; Bindi et al., 2009b).

The mainshock (event 1) was recorded by 57 stations in the epicentral distances range from 1.7 km to about 276 km with Joyner-Boore distances (R_{JB}) ranging from 0 to 266 km. In particular, there are 9 records with epicentral distances less than 30 km and 5 records with $R_{JB} = 0$. The largest PGA

(PGV) is 646 cm/s^2 (43 cm/s) recorded at station AQV; in general all PGAs recorded at epicentral distance less than 5km are greater than 350 cm/s^2 and the PGVs greater than 30 cm/s.

The two strongest aftershocks (event 2 and event 3), M_w=5.6 and M_w=5.4, were recorded by 44 and 35 stations respectively, with most of them located at epicentral distances less than 60 km. In particular, the event 2 and the event 3 were recorded by 12 and 9 stations within 16 km to the epicenter, respectively.

The maximum PGA and PGV from event 2 are 674 cm/s^2 and 23.5 cm/s, respectively, recorded at the closest station MI05, sited at 5.3 km from the epicenter. The maximum recorded PGA and PGV from event 3 are 177.6 cm/s^2 and 8.2 cm/s, respectively, recorded by GSA station at the epicentral distance of 16 km.

Figure 3b shows the vertical-to-horizontal PGA ratio (considering the geometric mean of the horizontal components) for the three events, grouping the peak values according to the distance. Values typically range between 0.25 and 0.75, and the rule-of-thumb of a 2/3 ratio between vertical and horizontal PGA is on average satisfied. The observed ratios at stations with R_{JB} = 0 are larger than 1 confirming that, in the near-source region, the vertical ground motions may be of the same order or significantly exceed the horizontal ones (see e.g., Bozorgnia and Campbell, 2004). It is also worth noting that the ratio of vertical to horizontal ground motion amplitude may also depend on site conditions. For example, V/H ratio is larger than 0.8 at some stations (i.e., BRS and AVZ, both classified as class B) farther than 20km from epicenters, that are known to be affected by amplification of the vertical component (Bindi et al., 2009a).

A very simple characterization of the ground motions from the three events can be obtained computing the PGA-to-PGV ratio: low values signify records with low predominant frequencies, broader response spectra and longer duration (Kwon and Elnashai, 2006). Figure 3c shows the PGA-to-PGV ratio (geometric mean of horizontal components) for the three events computed considering stations at distance less than 100 km. As expected, the two weaker events have similar distributions, while the mainshock records are characterized by higher low-frequency energy. The

mean PGA-to-PGV ratio (Table 3), computed for the recordings of the entire data set are (0.71± 0.4) g/ms^{-1} for event 1, (1.48± 0.8) g/ms^{-1} for event 2 and (1.9± 1.1) g/ms^{-1} for event 3. Following the classification by Zhu et al. (1988) and Kwon and Elnashai (2006), the main shock can be classified as an High Velocity-Low Acceleration earthquake (HV-LA: PGA-to-PGV < 0.8g/m s^{-1}). Interestingly, these ratios assume the lowest values when large distance records are included (i.e., > 20 km), while the PGA-to-PGV ratios of the near-source recordings are about 1. The same trend is observed for the two aftershocks.

In Figure 4a the observed PGAs and PGVs (maximum between the horizontal components) for the three events are plotted as a function of distance and compared with those estimated from national (ITA08, Bindi et al., 2009b) and global (BAT08, Boore and Atkinson, 2008) empirical ground motion prediction equations, and here used as references (Figure 4a). Formally the BAT08 equation is developed for an orientation independent measure of ground motion. We used the relationships proposed by Beyer and Bommer (2006) toconvert the BAT08 median estimates to the maximum horizontal component of motion for consistency with the other GMPEs.

On average and especially for the two aftershock, the PGVs are fitted by the empirical curves while the PGAs decay faster (particularly at distances larger than 20 km). The peak ground motions for the main event show a more complex trend: observed PGA and PGV at short distances agree with BAT08 and exceed the ITA08 predictions, as this GMPE is based on a data set that poorly samples the near-fault distances. At larger distances, the observed data are scattered with some of the data following the median trend of the GMPEs (computed for Mw = 6.3), while others seem better agree with the median curve for Mw = 5.4. This feature has been previously recognized by other authors (Ameri at al., 2009), showing that the L'Aquila mainshock ground motion is strongly azimuthally dependent. In particular these authors found that, for distances from 10 to about 100 km and for all site classes, the data east to the epicenter (roughly azimuths form 0° to 180°) follow the median trend estimated by the GMPEs, while the sites located in the western sector (180° to 360°)

are less than the median minus one standard deviation. They also suggested that this asymmetry in attenuation of PGA may be both ascribed to source and path effects.

To better understand the attenuation of ground motion in L'Aquila region, the residuals, defined as the logarithm difference between observations and predictions, are plotted as a function of distance, grouping the data for site classes (Figure 4b). The observed PGAs for the three site classes are constantly lower than the predicted values for distance larger than 25km, especially in case of global attenuation model. On the hand, residuals for PGV are between plus/minus 0.5 and no dependence on distance and site condition is observed. These results suggest that the high-frequency ground motion in the L'Aquila region decay faster with respect to the average trends described by national and global GMPEs.

4. Spatial distribution of ground motion

An overview of the spatial variability of ground motion recorded in the epicentral area during the 6 April earthquake and the two aftershocks is illustrated in Figure 5**,** where the distributions of the residuals between observed and predicted acceleration response spectra (at 5% damping) are plotted. To compute the residuals, the empirical ground motion prediction equation developed for Italian territory is adopted (ITA08, Bindi et al., 2009b) at periods 0.1s and 2s, considering appropriate site classes and distance up to 100km from the epicenters.

For the mainshock (Figure 5a), the positive residuals (observations larger than predictions) are mainly localized south-east to the epicenter, especially for long-period motions. Conversely negative residuals are found at short and long periods in the North-western area. Clear trends in the high-frequency residuals are found also in case of event 2 and event 3. For both, an evident underestimation of the observed spectral ordinates at T = 0.1s appears in the western sector (i.e., toward the Tyrrhenian Sea), whereas overestimation is observed the opposite sector (i.e., Adriatic Sea). At long period, for event 2, the absolute values of residuals are, in general, lower than 0.5 except for some sites in the Aterno Valley. On the other hand, for event 3, the regional distribution

of the long-period residuals is characterized by an asymmetric shape, with a clear underestimation area (i.e., positive residuals) elongated in the southeast direction respect to the epicenter. For the three earthquakes, the highest positive long-period residuals always occurred at AQK and CHT stations, both affected by strong site amplification at low frequency (< 1Hz).

The asymmetric regional distribution of residuals can be ascribed both to source and path effects. Directivity effects due to the rupture propagation over the fault can cause large variability of ground motion due to amplification in the direction toward which the rupture propagates (forward directivity) and de-amplification in the opposite (backward directivity) (e.g., Somerville et al., 1997). On the other hand, different seismic waves attenuation properties of the Earth crust can also be responsible for the azimuthal variability of residuals. Indeed the different attenuation between the eastern and western Apennines sectors has been observed (Mele et al., 1997). Evident forward and backward directivity effects have been recognized for the mainshock by the analysis of the instrumental and macroseismic data (Akinci et al., 2010; Pino and Di Luccio, 2009; Cirella et al., 2009; Ameri at al., 2010), caused by the fast quasi-unilateral rupture propagation toward South-East direction along the seismogenic fault. Propagation properties and seismic wave attenuation at regional scale should be investigated in order to explain the difference between the distribution of the short period residuals in the western region with respect to the eastern one.

The large variability of ground motion in the epicentral area is highlighted when recordings at stations, located at comparable distances from the epicenter but at different azimuths, are compared (Figure 6). The accelerogram (EW component) of mainshock recorded at ANT station, lying west to the epicenter, shows lower amplitudes than that at the eastern station CLN. Furthermore, larger amplitudes are found southward, as shown by the AVZ and MTR recordings, placed in opposite directions with respect to the epicenter. Also the strong-motion data recorded during event 2 and 3 show differences in amplitude depending on their azimuths. Examples are the recordings at CHT and SBC stations located at epicentral distance of about 50 km, but in the eastern and western sectors, respectively, and, for event 3, the BZZ and ANT recordings at sites placed at southeast or

northwest to the epicenter. Site effects also play an important role in defining some characteristics of the ground motion. An example is the large spectral ordinate at T = 1.5s of the acceleration response spectra observed at AVZ, installed close to the edge of the Fucino Basin.

5. Characteristics of near-source records

The stations of the Aterno array (Figure 2) are located within the surface projection of the L'Aquila mainshock fault and are at distances less than 5 km from the mainshock epicenter (Figure 1) and provide, together with the AQK and AQU stations, high quality near-fault strong-motion recordings.

Ameri et al. (2009) showed that velocity pulses are present at the beginning of all records and to a larger extent on AQK. Such pulses are due to the rupture propagation toward the sites at a velocity that is close to that of the shear-waves causing most of the seismic radiation from the fault to arrive compressed in time (Somerville et al., 1997). The radiation pattern of the shear dislocation on the fault causes this large pulse of motion to be oriented in the direction perpendicular to the fault, resulting in larger ground motions in the strike-normal (SN) direction than in the strike-parallel (SP) direction at periods longer than about 0.5 s (Somerville, 2003; Brady and Rodriguez-Marek, 2004). In the case of dip slip faults (as for the L'Aquila mainshock fault), near-source directivity pulses are expected for sites located above the fault, in the up-dip direction and close to the surface termination of the fault. Previous studies showed that the use of PGV is adequate as the representation of the amplitude of the velocity pulse in the time domain (Mavroeidis and Papageorgiou, 2003; Brady and Rodriguez-Marek, 2004) and larger PGV are typically observed in the strike-normal direction.

We investigated the PGV of AQA, AQV, AQG, AQK and AQU corrected records as a function of sensor orientation, in order to indentify the direction of maximum amplitude of the velocity pulses. Figure 7a shows the normalized PGVs obtained by rotating the NS time series over all non-redundant rotation angles. Several comments can be made. First, there is a substantial variation in PGV respect to the as-recorded values, represented by 0 and 90 rotation angles. For instance, the

PGV in the EW direction recorded at AQU station is about the 60% of the maximum horizontal PGV. As we do not know what will be the source-to-sensor azimuth for future earthquake we have to be aware that the near-fault ground motions recorded in the standard directions (i.e., NS and EW) can be substantially different to that on other horizontal directions. To account for this limitation, recently, orientation independent ground-motion intensity measures have been proposed in the context of ground motion prediction equations (Boore et al., 2006). Second, the direction of maximum PGV coincides surprisingly well, for all sites, with the SN direction (43°) when a fault strike of 133° is considered (as reported by Cirella et al., 2009). On the other hand the direction of minimum PGV coincides, as expected, with the SP direction (Somerville et al., 1997). Note that this feature is more evident for AQK and AQU records. Third, there are systematic differences between the three stations of the Aterno-Valley array (AQG, AQA and AQV) and the two stations located at L'Aquila city (AQK and AQU). The latter two present a clear maximum PGV in the SN direction and a minimum in the SP direction, which is 60-70% smaller than the maximum value. For the other three stations, a local maximum is visible at about 90°-110°.

In order to investigate whether such differences are due to different site amplification effects at the array stations, we filtered the records with a band-pass filter between 0.7 and 1.5 Hz and calculated the PGVs from rotated time series (Figure 7b). The choice of cut-off frequencies aims to emphasize the source-related pulses and to minimize the effects of local site conditions. The site effects at the three Aterno array stations show, in general, amplification peaks at frequencies higher than 1-2 Hz, whereas AQK and AQU stations are characterized by amplification peaks at about 0.6 Hz. (see Figure 2 and Ameri et al., 2009; Bindi et al., 2009a). On the other hand, the pulses period is generally recognized to be around 1s, at least in the strike-normal direction (Paolucci and Smerzini, 2010; Chioccarelli and Iervolino, 2010).

Figure 7b shows that for AQK and AQU records the direction of maximum and minimum PGVs are still in good agreement with the SN and SP directions, respectively (though small deviations are observed for the maximum PGV of AQU and the minimum of AQK). On the other hand AQG,

AQA and AQV stations show a different distribution of PGV as a function of rotation angle respect to what observed in Figure 7a and the local maximum/minimum PGVs disappear. In particular, AQV record presents the maximum and minimum PGVs close to the SP and SN direction, respectively, conversely to what observed for the other records. As AQV station is located at the center of the Aterno Valley there is the suspect that directionality in site amplification might influence the direction of maximum PGV presented in Figure 7b.

Figure 8 shows the velocity time series, recorded at the five near-source stations, rotated in the SN (43°) and SP (133°) directions for both 0.1-30 Hz (Figure 8a) and 0.7-1.5 Hz (Figure 8b) band-pass filters. For AQG, AQA and AQV stations, pulses are visible at the beginning of the records in both SN and SP direction, and the PGVs are comparable in the two directions (though the SN PGV is still to some extent larger). On the contrary for AQK and AQU, pulses are clearly visible only on the SN directions, whereas the amplitude of the SP time series is substantially smaller.

The very large amplitude of the pulse in the SN direction of the AQK record, compared to AQU, is most likely a result of a complex coupling of the source mechanism and the deep structure of the Aterno basin, where the lacustrine sediments reach around 250 m depth right underneath L'Aquila, as previously mentioned. This is confirmed by the filtered time series (Figure 8b), that show almost identical SN pulses for both AQK and AQU stations.

It is interesting to note that the strike-normal PGV for AQV record is not given by the first pulse in the time series (that is larger in the SP direction), but by a second pulse, with a shorter period, visible only in the FN direction. Such second pulse disappears when filtered time series are considered (Figure 8b), leading to a large velocity pulse in the FP direction, in according to what observed in Figure 7b.

Pulse-type records are of great interest to structural engineering because the seismic action in expected to be peculiar with respect to ordinary records. Indeed the elastic demand of pulse-like signals is generally larger than that of ordinary recordings, particularly concerning the SN direction. Moreover, the spectral shape is non-standard with an increment of spectral ordinates in the range

around the pulse period and, because the pulse period is generally at low frequencies (comparable to fundamental period of most of common structures), the inelastic demand can be particularly high and develop in comparatively short time (Tothong and Luco, 2007; Chioccarelli and Iervolino, 2010).

In Figure 9 the elastic spectral acceleration (SA) and spectral displacement (SD), at 5% damping, are presented for SN and SP components of AQA, AQK and AQU records. The spectral acceleration demand at short period (< T= 0.2s) is similar for both SN and SP motions, whereas at longer periods the spectral ordinates are systematically higher in the SN directions. This is particularly evident when looking at spectral displacement where the SN ordinates are remarkably larger than the SP ones.

6. Conclusions

The 6 April 2009 L'Aquila M_W 6.3 earthquake and its aftershocks yielded the most extensive set of digital strong-motion data, in particular in the near-source region, ever obtained in Italy. The mainshock and the two following largest events provide more than 130 three-components strong-motion records, with about 90 records within 100 km of the corresponding epicenters.

The analysis of the observed peak ground motion and their ratios (vertical-to-horizontal components and peak ground velocity-to peak ground acceleration) allows us to highlight some important features on the recorded ground motion in epicentral area.

A faster decay with distance of the high-frequency respect to the low-frequency radiation is observed, leading to classify the Abruzzo earthquake as a High Velocity-Low Acceleration event. The residuals of spectral ordinates at 0.1s and 2s, computed with respect to empirical predictions show a clear dependence on azimuth, that can be attributed both to source effects (i.e., directivity effects) and to different attenuation properties of seismic waves at crustal scale. In particular, for the three events, a clear underestimation of the short-period ground motion appears west to the Apennine chain, whereas overestimation is observed the opposite sector (i.e., towards the Adriatic

Sea), in agreement with the different shear-wave attenuation reported for the two zones in literature (e.g., Mele et al., 1997). Site effects also play an important rule in explaining the observed ground motion variability.

The analyses of mainshock near-fault records show that peak motion varies significantly for stations within 5 km from the epicentre, spanning from the 0.66 g, recorded at AQV, to 0.26g at AQU. All these recordings are characterized by near-source velocity pulses with periods around T = 1s, having maximum amplitude oriented in the direction perpendicular to the fault strike.

However, there are systematic differences in the strike-normal and strike-parallel velocities between the three stations of the Aterno-Valley array (AQG, AQA and AQV) and the two stations located at L'Aquila city (AQK and AQU). In the former, velocity pulses of comparable amplitude are visible in both strike-normal and strike-parallel directions, while, in the latter they are clearly visible only in the strike-normal direction. This study suggests that their amplitude and orientation, in the case of the array sites, is influenced also by the Aterno Valley site effects.

Finally we emphasize that because of the near-fault conditions, the complex geological setting and the availability of several good-quality near-fault records, this earthquake resulted in an important benchmark that provided an impressive and instructive picture of strong ground motion in the epicentral region of a normal fault earthquake.

Acknowledgements

This work has been partly supported by the Italian Department of Civil Protection under Project S4, Italian strong-motion database, within the DPC-INGV 2007-09 agreement. The insightful comments and suggestions of Aldo Zollo and an anonymous reviewer helped improve the quality of the paper.

References

Akkar, S. and Bommer, J.J., 2007. " Prediction of elastic displacement response spectra in Europe and the Middle East," *Earthquake Engineering and Structural Dynamics* , 36, 1275-1301

Akinci, A., Malagnini, L. and Sabetta, F. 2010. Characteristics of the strong ground motions from the 6 April 2009 L'Aquila earthquake, Italy. *Soil Dyn. Earthquake Eng*, 30, 320-335.

Ameri G., Bindi D., Pacor F. and F. Galadini (2010). The 6 April 2009, M_w 6.3, L'Aquila (Central Italy) earthquake: directivity effects on intensity data, *submitted to Geoph. J. Int.*

Ameri G., Massa M., Bindi D., D'Alema E., Gorini A. Luzi L., Marzorati S., Pacor F., Paolucci R., Puglia R. and C. Smerzini (2009). The 6 April 2009, M_w 6.3, L'Aquila (Central Italy) earthquake: strong-motion observations, *Seismological Research Letters*, 80, 6; 951-966.

Beyer, K., and JJ. Bommer (2006). Relationships between median values and between aleatory variabilities for different definitions of the horizontal component of motion, *Bulletin of the Seismological Society of America*, 96, 1512-1522.

Bindi D., Pacor F., Luzi L. Massa M. and G. Ameri (2009a). The Mw 6.3, 2009 L'Aquila earthquake: source, path and site effects from spectral analysis of strong motion data, *Geoph. J. Int.*, 179, 1573–1579.

Bindi, D., L. Luzi, M. Massa, and F. Pacor (2009b). Horizontal and vertical ground motion prediction equations derived from the Italian Accelerometric Archive (ITACA). *Bulletin of Earthquake Engineering*; doi:10.1007/s10518-009-9130-9.

Boore, D. M., J. Watson-Lamprey, and N. A. Abrahamson (2006). GMRotD and GMRotI: Orientation-independent measures of ground motion. *Bulletin of the Seismological Society of America* 96, 1,502–1,511.

Boore, D.M. and G.M. Atkinson (2008). Ground-Motion Prediction Equations for the Average Horizontal Component of PGA, PGV, and 5%-Damped PSA at Spectral Periods between 0.01s and 10.0s, *Earthquake Spectra,* 24, 99-138.

Bosi C., Galadini F., Giaccio B., Messina P. and A. Sposato (2003). Plio-Quaternary continental deposits in the Latium-Abruzzi Apennines: the correlation of geological events across different intermontane basins, *Il Quaternario,* 16, 55-76.

Bozorgnia Y. and K.W. Campbell (2004). The vertical to horizontal response spectral ratio and tentative procedures for developing simplified V/H and vertical design spectra, *Journal of Earth. Eng.,* 8(2), 175-207.

Bray, J. D., and A. Rodriguez-Marek (2004). Characterization of forward-directivity ground motions in the near-fault region. *Soil Dynamics and Earthquake Engineering* 24, 815–828.

Camassi,R., P. Galli, A. Tertulliani, S. Castenetto, A. Lucantoni, D. Molin, G. Naso, E. Peronace, F. Bernardini, V. Castelli, A. Cavaliere, E. Ercolani, S. Salimbeni, D. Tripone, G. Vannucci, L. Arcoraci, M. Berardi, C. Castellano, S. Del Mese, L. Graziani, I. Leschiutta, A. Maramai, A. Massucci, A. Rossi, M. Vecchi, R. Azzaro, S. D¹Amico, F. Ferrari, N. Mostaccio, R. Platania, L. Scarfì, T. Tuvé, L. Zuccarello, S. Carlino, A. Marturano, P. Albini, A. Gomez Capera, M. Locati, F.

Meroni, V. Pessina, C. Piccarreda, A. Rovida, M. Stucchi, G. Buffarini, S. Paolini, V. Verrubbi, M. Mucciarelli, R. Gallipoli, M.S. Barbano, I. Cecic, M. Godec (2009). L'indagine macrosismica: metodologia, parametri del terremoto, questioni aperte. *Progettazione Sismica*, 3, 49 -55.

Comité Européen de Normalisation (CEN) (2004). *Eurocode 8: Design of Structures for Earthquake Resistance—Part 1: General Rules, Seismic Actions and Rules for Buildings*. Brussels: Comité Européen de Normalisation.

Chiarabba, C. *et al.* 2009. The 2009 L'Aquila (central Italy) M_W6.3 earthquake: Main shock and aftershocks, *Geophys. Res. Lett*., 36, L18308, doi:10.1029/ 2009GL039627.

Chioccarelli, E., and I., Iervolino (2010). Near-source seismic demand and pulse-like records: A discussion for L'Aquila earthquake. *Earthquake Engng Struct. Dyn*, DOI: 10.1002/eqe.987

Cirella A., A. Piatanesi, M. Cocco, E. Tinti, L. Scognamiglio, A. Michelini, A. Lomax, E. Boschi (2009). Rupture history of the 2009 L'Aquila (Italy) earthquake from non-linear joint inversion of strong motion and GPS data, *Geophysical Research Letters,* Vol. 36, L19304.

De Luca G., S. Marcucci, G. Milana, T. Sanò (2005). Evidence of low-frequency amplification in the city of L'Aquila, Central Italy, through a multidisciplinary approach, *Bull. Seism. Soc. Am.,* Vol. 95, pp. 1469-1481.

Falcucci, E., S. Gori, E. Peronace, G. Fubelli, M. Moro, M. Saroli, B. Giaccio, P. Messina, G. Naso, G. Scardia, A. Sposato, M. Voltaggio, P. Galli, & Galadini, F., 2009. The Paganica fault and surface coseismic ruptures caused by the 6 April 2009 earthquake (L'Aquila, central Italy). *Seismological Research Letters* 80 (6), 940–950.

Galli P. and Camassi R. (eds.), 2009. Rapporto sugli effetti del terremoto aquilano del 6 aprile 2009, Rapporto congiunto DPC-INGV, 12 pp. Available at: http://portale.ingv.it/real-time-monitoring/quest/aquilano-06-04-2009/).

Gruppo di Lavoro MPS (2004). Redazione della mappa di pericolosità sismica prevista dall'Ordinanza PCM del 20 marzo 2003. Rapporto Conclusivo per il Dipartimento della Protezione Civile, INGV, Milano-Roma, 65 pp. + 5 appendici. *In Italian*

Kwon O.S. and A. Elnashai (2006). The effect of material and ground motion uncertainty on the seismic vulnerability curves of RC structure, *Engineering Structures*, 28, 289–303.

Lermo J. and F. Chavez-Garcia (1993). Site effect evaluation using spectral ratio with only one station, *Bull. Seism. Soc. Am.*, 83, 5, 1574-1594.

Luzi L., Hailemikael S., Bindi D., Pacor F., Mele F. and F. Sabetta (2008). ITACA(ITalian Accelerometric Archive): a web portal for the dissemination of Italian strong-motion data, *Seismol. Res. Letters,* 79, 716-722.

Mavroeidis, G. P., and A. S. Papageorgiou (2003). A mathematical representation of near-fault ground motions, *Bull. Seism. Soc. Am.* 93**,** 1099–1131.

Mele G., Rovelli, A., Seber, G. and M. Barazangi (1997) Shear wave attenuation in the lithosphere beneath Italy and surrounding regions: tectonic implications, *J. Geophyis. Res.*, 102, B6, 11,863-11,865.

Norme Tecniche per le Costruzioni (2008). DM 140108, Ministero delle Infrastrutture, Roma, Gazzetta Ufficiale.

Paolucci R., Pacor F., Puglia R., Ameri G., Cauzzi C. and M. Massa (2010). Record processing in ITACA, the new Italian strong-motion database . 2nd Euro-Mediterranean meeting on accelerometric Data Exchange and Archiving, *Springer, Editor: S. Akkar and P. Gulkan*. *Accepted*

Paolucci R., and C. Smerzini (2010), Strong ground motion in the epicentral region of the Mw 6.3, Apr. 6 2009, L'Aquila earthquake, Italy. *Fifth International Conference on Recent Advances in Geotechnical Earthquake Engineering and Soil Dynamics*, San Diego, California, May 24-29, 2010

Pino, N.A. and F., Di Luccio (2009), Source complexity of the 6 April 2009 L'Aquila (central Italy) earthquake and its strongest aftershock revealed by elementary seismological analysis, *Geophys. Res. Lett.*, 36, L23305, doi:10.1029/2009GL041331.

Somerville PG, Smith NF, Graves RW, Abrahamson NA. (1997). Modification of empirical strong motion attenuation relations to include the amplitude and duration effect of rupture directivity. *Seismological Research Letters*; 68(1):199–222.

Somerville, P.G. (2003). Magnitude scaling of the near fault rupture directivity pulse. *Physics of the Earth and Planetary Interiors*; 137:201–212.

Tothong P, Luco N. (2007).Probabilistic seismic demand analysis using advanced ground motion intensity measures. *Earthquake Engineering and Structural Dynamics*; 36:1837–1860.

Zhu TJ, Heidebrecht AC, Tso WK. (1988) Effect of peak ground acceleration to velocity ratio on ductility demand of inelastic systems. *Earthq Eng Struct Dyn*;16:63–79.

Figure caption

Figure 1 - Location of the main events (M_w > 4) of the L'Aquila sequence (red stars) and of the accelerometric stations belonging to RAN (dots) and to INGV MI-PV (triangles). The surface projection of the fault is also shown (Falcucci et al., 2009). Focal mechanisms are shown for the three strongest events.

Figure 2 – Upper panel: location of the strong motion stations of the Aterno Valley array and of AQK and AQU, plotted on local geology. The star indicates the mainshock epicenter. Lower panel: horizontal to vertical spectral ratios (HVSR), calculated at 5 stations (for both horizontal components) using the mainshock and 12 aftershocks of the L'Aquila seismic sequence, are shown as dashed lines (grey area indicates the ± 1 standard deviation). Empirical site response for horizontal (black line) and vertical (grey line) components estimated through generalized inversion technique by Bindi et al. (2009a) are also reported.

Figure 3 - a) Magnitude – distance distribution of the strong-motion data recorded by the three strongest event of the L'Aquila seismic sequence. The data are grouped according to the EC8 classes (grey diamonds for class A, crosses for class B, circles for class C). Note that points with R_{JB}=0 are plotted at 0.1 km. b) Ratio between the Horizontal (geometric mean) and Vertical peak ground acceleration (PGA) for the 06-04-2009 event (1), 07-04-2009 event (2) and the 09-04-2009 event (3). c) Ratio between the Horizontal (geometric mean) peak ground acceleration and velocity (PGA/PGV) for the 06-04-2009 event (1), 07-04-2009 event (2) and the 09-04-2009 event (3).

Figure 4 – a) Maximum horizontal peak ground acceleration (left) and velocity (right) versus distance up to 100 km. The red and grey lines show the predictions computed by the Italian and global empirical ground motion prediction equations (ITA08, Bindi et al., 2009b; BAT08, Boore and Atkinson, 2008) for rock sites and magnitude Mw 6.3 and 5.4. Observed peak values are

indicated with diamonds for event1 (06-04-2009), grey circles for event2 (07-04-2009) and black circles for event3 (09-04-2009) .

b) Residuals versus distance for PGA (right) and PGV (left). The residuals are computed using the ITA08 (top) and the BAT08 (bottom) predictions. An equivalent EC8 class is used for the GMPEs . For ITA08 class 0 corresponds to A (red crosses), class 1 to B (grey diamonds) and class 2 to C (circles). For BAT08 model, Vs30 = 900 m/s is assigned for class A; Vs30 =537 m/s for class B and Vs30 = 255 m/s for class C

Figure 5 - Spatial distribution of the residuals. For each site residuals are calculated as $\log_{10}$(observed/predicted) where the Italian empirical ground motion prediction equation (ITA08, Bindi et al., 2009b) is used for each specific site classes. Red circles indicate underestimation, while blue squares indicate overestimation. The residual are computed for the maximum spectral acceleration at 0.1s (left) and 2 s (right) for event 1 (a) event 2 (b) and event 3 (c).

Figure 6 – Examples of acceleration time series in cm/s^2 (EW component) and acceleration response spectra (EW component: black; NS component: grey) recorded during event 1, event 2 and event 3 by some selected stations in epicentral area.(black triangles). The white stars indicate the location of the epicenters. Stations are located in the distance range from 18 to 60 km at difference azimuth with respect to the epicenters. For each station, the identification code, the site class, the recorded event and the epicentral distance are reported.

Figure 7 - Normalized Peak Ground Velocity (PGV) as a function of rotation angle for the five near-source mainshock recordings, considering 0.1-30 Hz (a) and 0.7-1.5 Hz (b) band-pass filtered time series. 0° and 90° represent the NS and EW direction (as-recorded PGVs). The vertical dashed lines are the strike-normal direction (44°) and strike-parallel direction (133°) according to the fault rupture model proposed by Cirella et al. (2009).

Figure 8 - Strike-Normal (black) and Strike-Parallel (gray) velocity time series at the five near-source stations, considering 0.1-30 Hz (a) and 0.7-1.5 Hz (b) band-pass filters. The labels report the PGV in the two directions (cm/s).

Figure 9 - Comparison of 5% damped acceleration (SA, left) and displacement (SD, right) response spectra along the SN (black) and SP (gray) components.

Table 1 - Main Source Parameters of the considered events

Date* yyyymmdd	**time (UTC)* hhmmss**	**Lat.(N)* [°]**	**Lon.(E)* [°]**	**H* [km]**	**Ml***	**Mw^{+}**	**Strike^{+} [°]**	**Dip^{+} [°]**	**Rake^{+} [°]**
20090406	013240	42.348	13.380	9.5	5.8	6.3	147.0 *133.0*	43.0 *54.0*	-88.0 *-102*
20090407	174737	42.275	13.464	15.1	5.3	5.6	109.0	51.0	-124.0
20090409	005259	42.484	13.343	15.4	5.1	5.4	148.0	40.0	-90.0

* from INGV-CNT Bulletin (Chiarabba et al., 2009); + from Regional Centroid Moment Tensor (http://www.bo.ingv.it/RCMT/)
In italic: fault mechanism from Cirella et al. (2009), note that reported rake angle corresponds to that associated to the maximum slip area on the fault.

Table 2 – Strong-motion stations installed in the area that recorded at least one of the three strongest events. Geographical coordinates, site class according to EC8 site classification, and the event recorded at each station are reported in the relative column.

Name	Code	Owner	Lat (°)	Long (°)	EC8	#events
Antrodoco	ANT	DPC	42.4181	13.0786	A*	1 2 3
L'Aquila F. Aterno	AQA	DPC	42.3755	13.3393	B	1 3
L'Aquila Ferriera	AQF	DPC	42.3805	13.3547	B*	2
L'Aquila Colle Grilli	AQG	DPC	42.3735	13.3370	B	1 2 3
L'Aquila Aquilpark	AQK	DPC	42.3450	13.4009	B	1 2 3
L'Aquila Il Moro	AQM	DPC	42.3786	13.3493	A*	2 3
L'aquila Monte Pettino	AQP	DPC	42.3837	13.3686	A	2 3
L'Aquila Castello	AQU	Mednet	42.3539	13.4019	B*	1 2 3
L'Aquila Centro Valle	AQV	DPC	42.3772	13.3439	B	1 2 3
Assisi	ASS	DPC	43.0750	12.6041	A*	1 2
Avezzano	AVZ	DPC	42.0275	13.4259	B*	1 2 3
Barisciano	BRS	DPC	42.3239	13.5903	B*	3
Bazzano	BZZ	DPC	42.3370	13.4686	B	2 3
Castel Di sangro	CDS	DPC	41.7871	14.1119	A*	1 2 3
Chieti	CHT	DPC	42.3698	14.1478	B	1 2 3
Celano	CLN	DPC	42.0852	13.5207	A*	1 2 3
Carsoli	CSO1	DPC	42.1009	13.0881	A*	1 2 3
Cassino	CSS	DPC	41.4858	13.8231	A*	1 2 3
Cattolica	CTL	DPC	43.9550	12.7360	B*	1 2
Fiamignano	FMG	DPC	42.2680	13.1172	A*	1 2 3
Gran Sasso Assergi	GSA	DPC	42.4207	13.5194	C*	1 2 3
Isernia	ISR	DPC	41.6106	14.2359	C*	1 2
Leonessa	LSS	DPC	42.5582	12.9689	A*	1 2 3
Pescomaggiore	MI01	INGV-MI	42.3580	13.5098	A*	2 3
Paganica	MI02	INGV-MI	42.3545	13.4743	C*	2 3
Onna	MI03	INGV-MI	42.3274	13.4757	B	2 3
S. Eusanio Forc.	MI05	INGV-MI	42.2895	13.5253	B*	2 3
Mompeo	MMP	DPC	42.2486	12.7486	A*	1 2 3
Montereale	MTR	DPC	42.5240	13.2448	A*	1 2 3
Ortucchio	ORC	DPC	41.9536	13.6423	A*	1 2 3
Pescasseroli	PSC	DPC	41.8120	13.7892	A	2 3
Subiaco	SBC	DPC	41.9132	13.1055	A*	1 2
Scanno	SCN	DPC	41.9187	13.8724	A*	2 3
Spoleto cantina	SPC	DPC	42.7435	12.7397	C*	1 2 3
Spoleto	SPO	DPC	42.7336	12.7406	A*	1 2 3
Sulmona	SUL	DPC	42.0890	13.9340	A*	1 2 3

Table 3 – PGA/PGV [g/m/s] values (mean ± standard deviation) calculated for the three events and grouping the data according to distance ranges or different site classification.

	event 1 [g/m/s]	**event 2** [g/m/s]	**event 3** [g/m/s]
All	0.71±0.40	1.48±0.80	1.90±1.05
< 20km	1.37±0.24	2.16±0.67	2.30±0.92
>20km	0.58±0.27	1.17±0.80	1.65±1.07
EC8 A	0.77±0.40	1.56±0.88	1.92±1.16
EC8 B	0.61±0.37	1.37±0.82	1.58±0.94
EC8 C	0.73±0.48	1.43±0.56	2.39±0.83

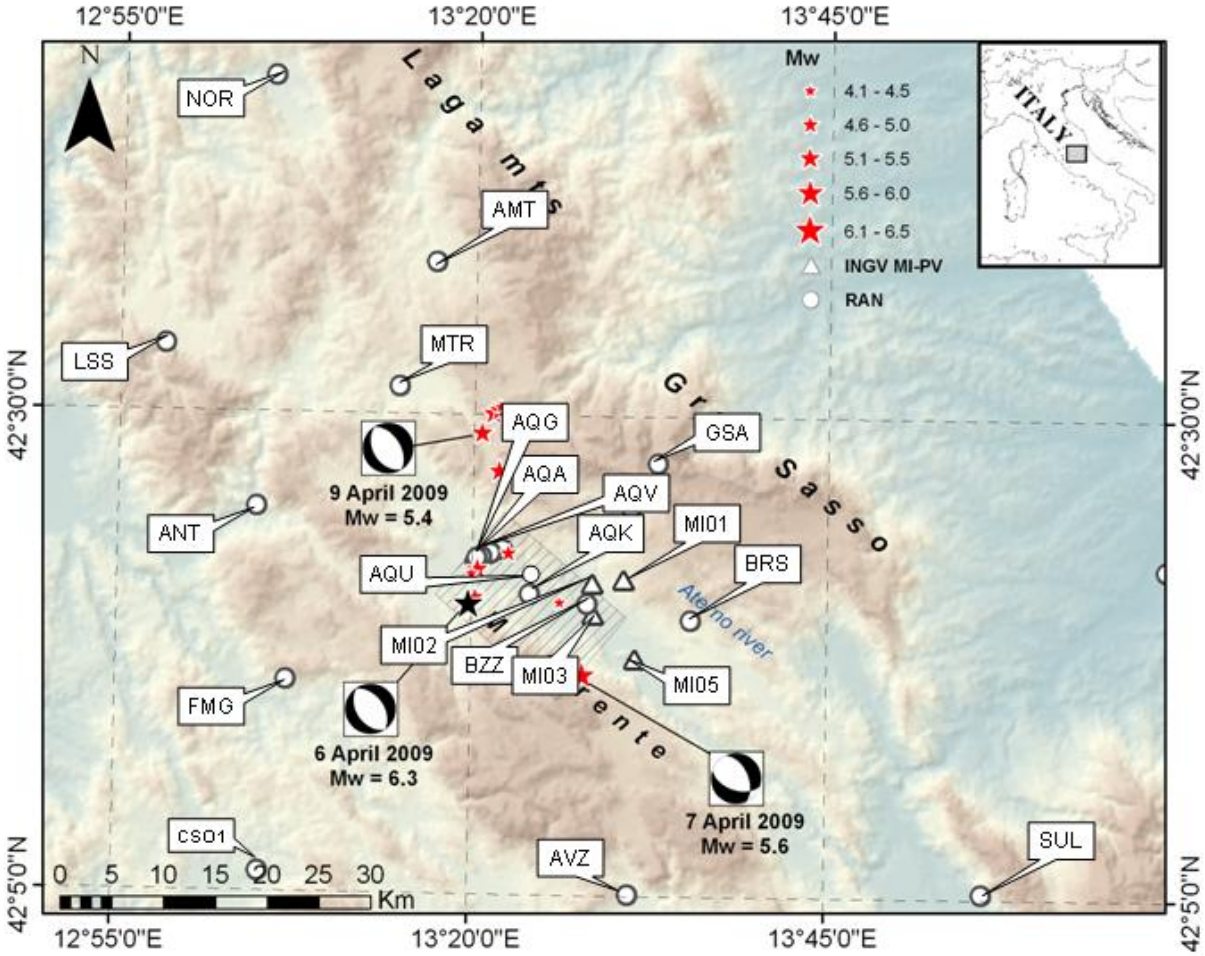
12°55'0"E
13°20'0"E
13°45'0"E
42°30'0"N
42°5'0"N
N
Mw
4.1 - 4.5
4.6 - 5.0
5.1 - 5.5
5.6 - 6.0
6.1 - 6.5
INGV MI-PV
RAN
ITALY
Laga mts
Gr Sasso
Aterno river
NOR
AMT
LSS
MTR
AQG
GSA
AQA
AQV
ANT
AQK
MI01
AQU
BRS
MI02
BZZ
MI03
MI05
FMG
CSO1
AVZ
SUL
9 April 2009
Mw = 5.4
6 April 2009
Mw = 6.3
7 April 2009
Mw = 5.6
0 5 10 15 20 25 30
Km

Figure 1

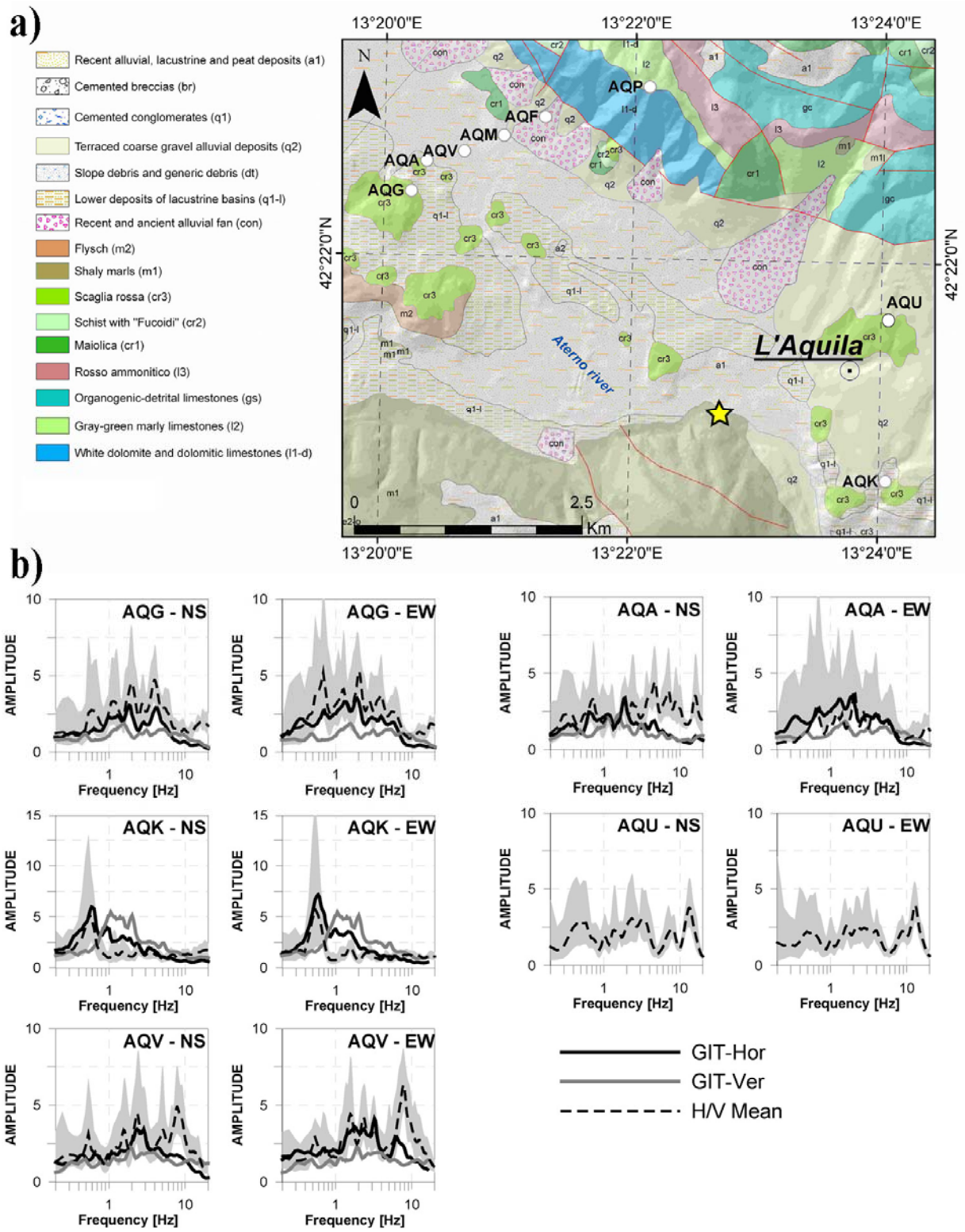
a)
Recent alluvial, lacustrine and peat deposits (a1)
Cemented breccias (br)
Cemented conglomerates (q1)
Terraced coarse gravel alluvial deposits (q2)
Slope debris and generic debris (dt)
Lower deposits of lacustrine basins (q1-l)
Recent and ancient alluvial fan (con)
Flysch (m2)
Shaly marls (m1)
Scaglia rossa (cr3)
Schist with "Fucoidi" (cr2)
Maiolica (cr1)
Rosso ammonitico (l3)
Organogenic-detrital limestones (gs)
Gray-green marly limestones (l2)
White dolomite and dolomitic limestones (l1-d)
13°20'0"E
13°22'0"E
13°24'0"E
42°22'0"N
N
AQP
AQF
AQM
AQV
AQA
AQG
AQU
L'Aquila
Aterno river
0
2,5
Km
b)
AQG - NS
AQG - EW
AQA - NS
AQA - EW
AQK - NS
AQK - EW
AQU - NS
AQU - EW
AMPLITUDE
Frequency [Hz]
GIT-Hor
GIT-Ver
H/V Mean

Figure 2

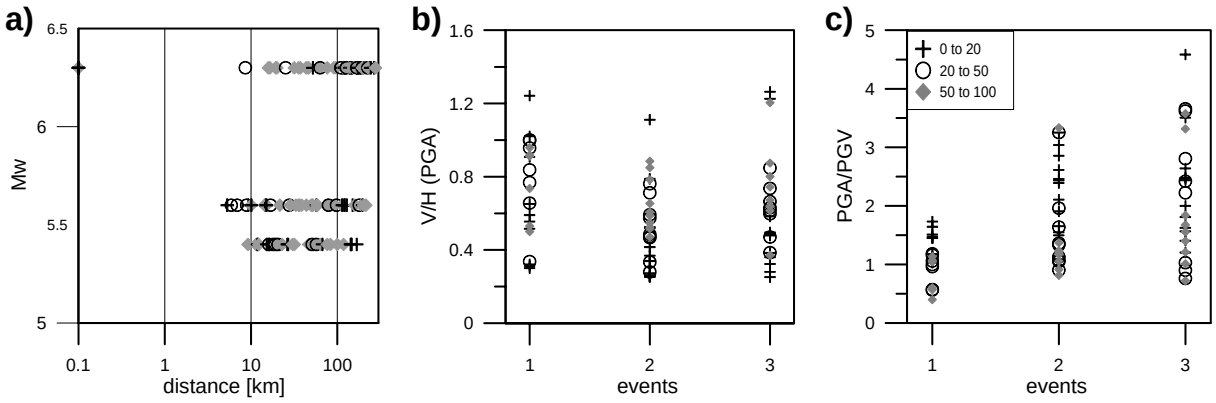
a)
Mw
6.5
6
5.5
5
0.1
1
10
100
distance [km]
b)
V/H (PGA)
1.6
1.2
0.8
0.4
0
1
2
3
events
c)
PGA/PGV
0 to 20
20 to 50
50 to 100
5
4
3
2
1
0
1
2
3
events

Figure 3

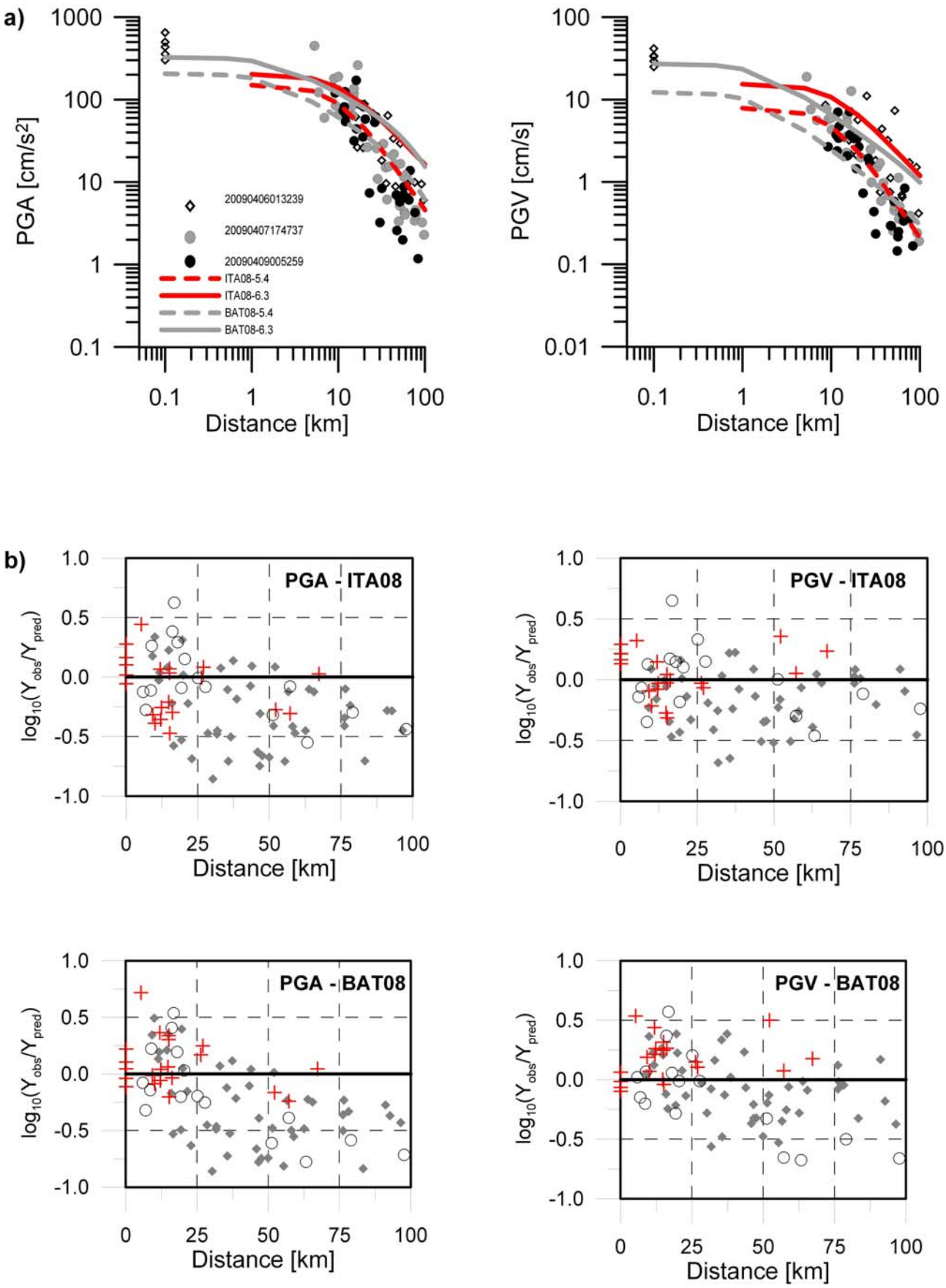
a)
PGA [cm/s²]
1000
100
10
1
0.1
0.1
1
10
100
Distance [km]
20090406013239
20090407174737
20090409005259
ITA08-5.4
ITA08-6.3
BAT08-5.4
BAT08-6.3
PGV [cm/s]
100
10
1
0.1
0.01
b)
PGA - ITA08
PGV - ITA08
PGA - BAT08
PGV - BAT08
log10(Yobs/Ypred)
1.0
0.5
0.0
-0.5
-1.0
0
25
50
75
100
Distance [km]

Figure 4

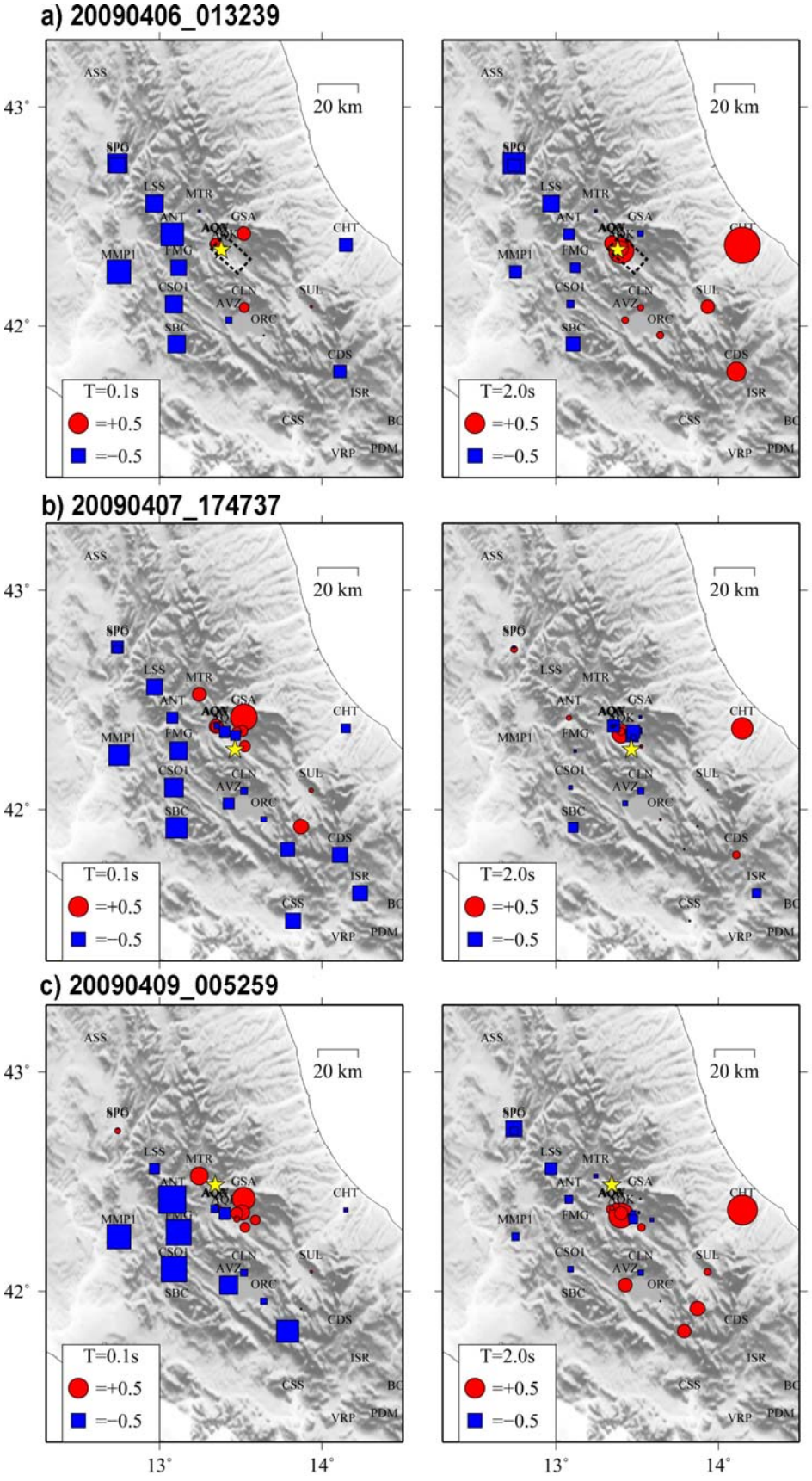
a) 20090406_013239
b) 20090407_174737
c) 20090409_005259
20 km
T=0.1s
T=2.0s
=+0.5
=−0.5
ASS
SPO
LSS
MTR
ANT
GSA
AQU
CHT
MMP1
FMG
CSO1
CLN
AVZ
SUL
ORC
SBC
CDS
ISR
CSS
BC
VRP
PDM
43°
42°
13°
14°

Figure 5

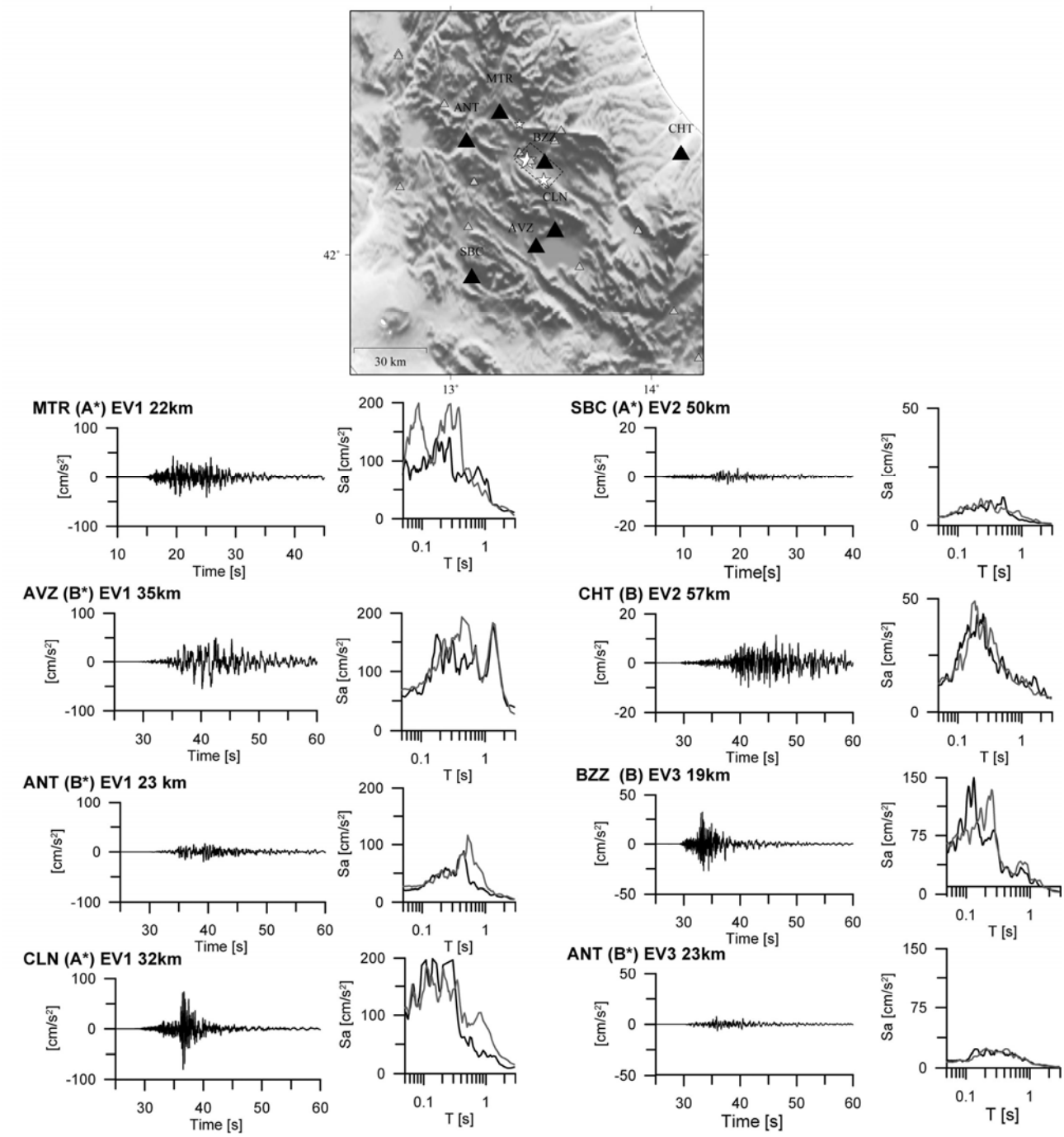
MTR
ANT
BZZ
CHT
CLN
AVZ
SBC
42°
30 km
13°
14°
MTR (A*) EV1 22km
SBC (A*) EV2 50km
AVZ (B*) EV1 35km
CHT (B) EV2 57km
ANT (B*) EV1 23 km
BZZ (B) EV3 19km
CLN (A*) EV1 32km
ANT (B*) EV3 23km
[cm/s²]
Sa [cm/s²]
Time [s]
T [s]

Figure 6

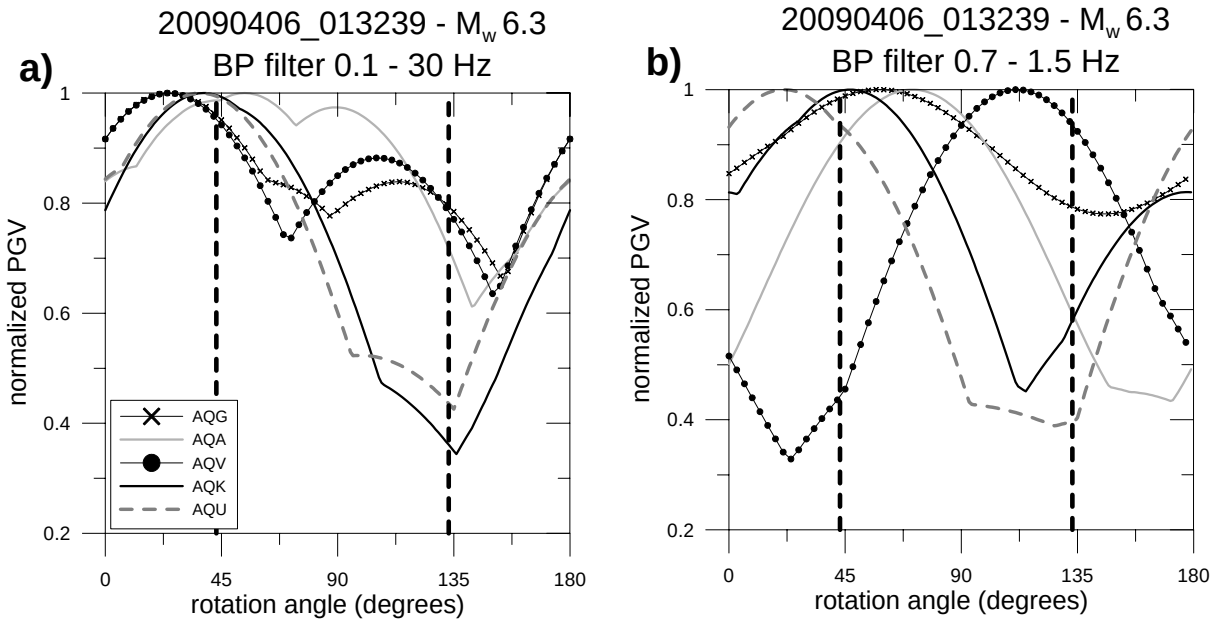
20090406_013239 - M_w 6.3
BP filter 0.1 - 30 Hz
a)
normalized PGV
rotation angle (degrees)
AQG
AQA
AQV
AQK
AQU
20090406_013239 - M_w 6.3
BP filter 0.7 - 1.5 Hz
b)
normalized PGV
rotation angle (degrees)

Figure 7

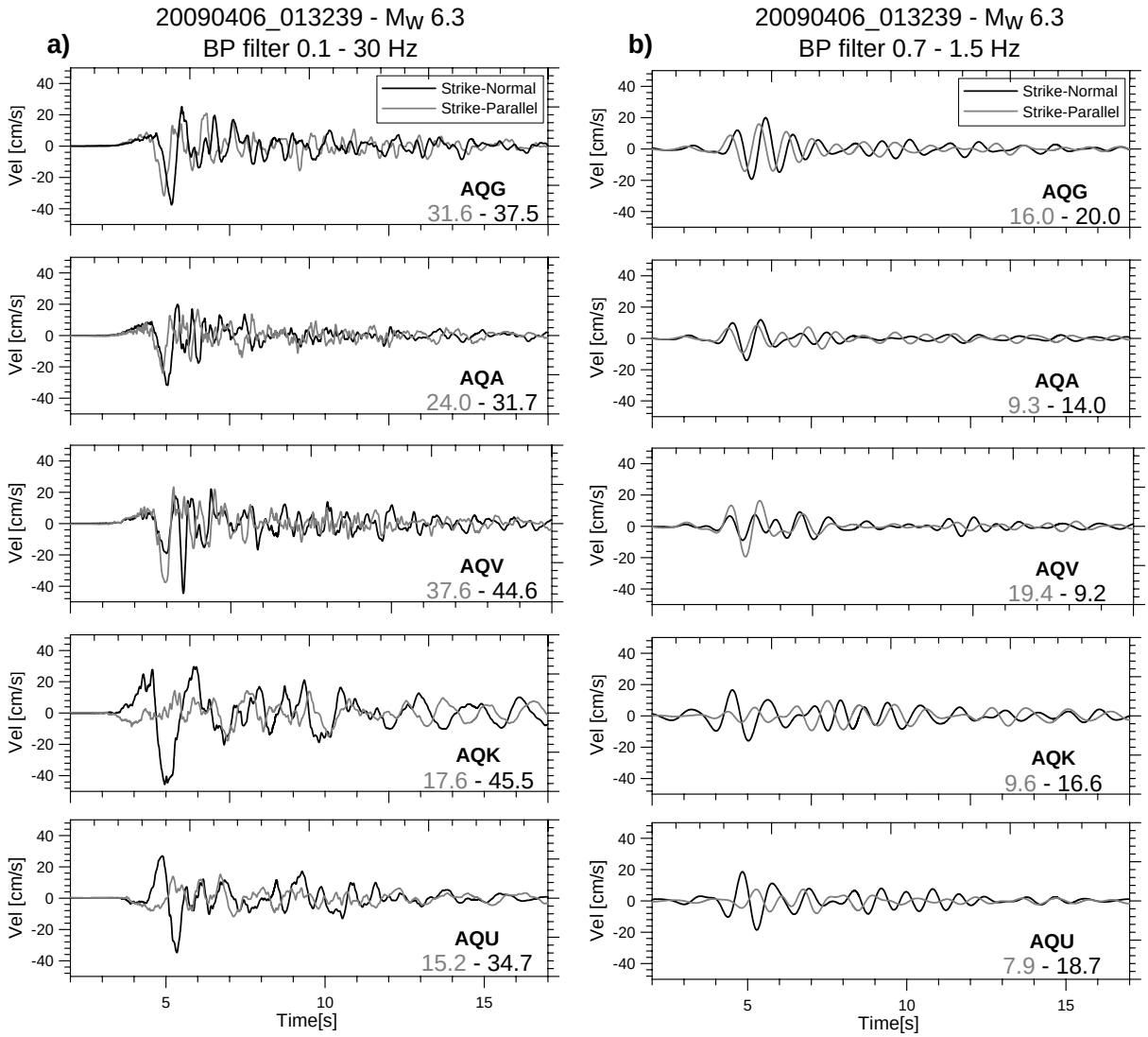
20090406_013239 - Mw 6.3
a)
BP filter 0.1 - 30 Hz
Strike-Normal
Strike-Parallel
Vel [cm/s]
AQG
31.6 - 37.5
AQA
24.0 - 31.7
AQV
37.6 - 44.6
AQK
17.6 - 45.5
AQU
15.2 - 34.7
Time[s]
20090406_013239 - Mw 6.3
b)
BP filter 0.7 - 1.5 Hz
AQG
16.0 - 20.0
AQA
9.3 - 14.0
AQV
19.4 - 9.2
AQK
9.6 - 16.6
AQU
7.9 - 18.7

Figure 8

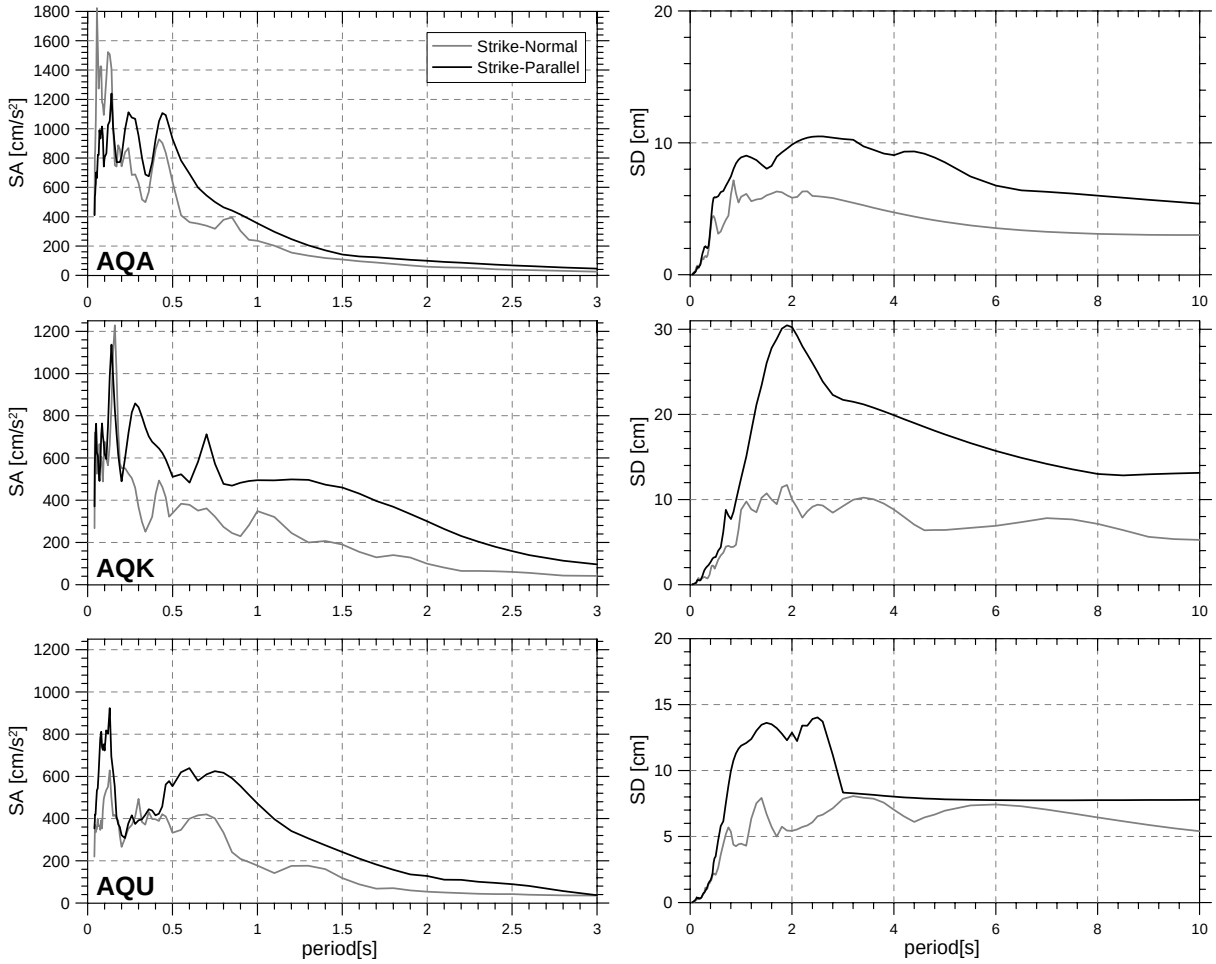
Strike-Normal
Strike-Parallel
SA [cm/s²]
SD [cm]
AQA
AQK
AQU
period[s]

Figure 9